Meas. Sci. Technol. **31** (2020) 084004 https://doi.org/10.1088/1361-6501/ab85d5

# Multi-camera Large-Scale Particle Image Velocimetry

**Ryota Tsubaki**[1]

[1] Graduate School of Engineering, Nagoya University, Furo-cho, Chikusa-ku, Nagoya 464-8603, Japan

E-mail: rtsubaki@civil.nagoya-u.ac.jp

Received 16 December 2019
Accepted for publication 2 April 2020
Published 25 May 2020

## Abstract

Large-scale particle image velocimetry (LSPIV) has been widely used for quantifying the velocity distribution of environmental water surfaces, especially river flows. In LSPIV, the evaluated velocity distribution of a region far from the camera tends to have a large uncertainty due to strong image distortion and reduced image resolution, especially for directions parallel to the viewing angle. This study proposes a method that overcomes this problem by combining the results of LSPIV measurements of images obtained from different viewing angles. The velocity component for the direction orthogonal to the viewing angle (the 1D velocity component) for each viewing angle was extracted and then the 2D velocity field was reconstructed based on a least squares algorithm. To validate the proposed method, a rigid rotating disk experiment and a circulatory flow flume experiment were conducted. The method was used to reproduce a complex flow formed around an opposite river edge using images obtained from two different locations on a river bank. Circulatory flow was not visible from results obtained from single viewing angles but was successfully represented in the reconstructed velocity field.

Keywords: Large-Scale Particle Image Velocimetry (LSPIV), image resolution, multi camera, viewing angle, low depression angle

(Some figures may appear in colour only in the online journal)

## 1. Introduction

The development and application of image-based stream flow measurements are active research challenges (e.g. Johnson & Cowen, 2017), not only in academic research but in practical applications for quantifying flow, for example, when estimating the discharge hydrograph for an experiment of dam breach (Bento et al. 2017) or the flow rate and water level in a remote area with limited human and economic resources (e.g. Strobl et al., 2019). Image-based stream flow observations (e.g. Large-Scale Particle Image Velocimetry: LSPIV) consist of three procedures: (i) image acquisition, (ii) ortho-rectification, and (iii) image-based velocity estimations (e.g. Fujita et al 2004; Tsubaki et al., 2015; Tauro et al., 2017). Figure 1 schematically explains the procedures of LSPIV. Ortho-rectification is a type of coordinate transform (e.g. Tsubaki et al., 2018) and is used in the 'PIV-later approach' shown in Figure 1. When ortho-rectifying a raster image, pixel interpolation is needed and causes the degradation of image resolution in areas far from the camera, and for the forward/backward directions. The distorted checker-board pattern in the bottom-right of Figure 1 correspondss to a distorted image resolution due to ortho-rectification. This distortion, especially notable in the area far from the camera and in the forward/backward direction, limits the accuracy and

 

precision of water surface velocity estimations. Other than the 'PIV-later approach', we can apply PIV to the acquired images and then transform the coordinate of the vectors. This approach is named the 'PIV-first approach' (e.g. Hauet A et al 2008). The result obtained from both approaches is identical if no errors in the PIV and coordinate transform exist. However, in practice, they are not identical due to non-negligible errors within the coordinate transform and the PIV, especially when a largely skewed coordinate transform is required.

To avoid larger distortions caused by ortho-rectification, structures (e.g. poles (Kim et al. 2008) or towers (Fujita et al 2004)) or maneuvering bodies (e.g. Unmanned Aerial Vehicles (e.g. Schoutheete et al 2019) or helicopters (e.g. Fujita and Kunita 2011)) have been used to locate the camera at a high altitude and to make the depression angle almost orthogonal. Such an approach has been implemented using manual particle seeding. Water surface ripples generated by turbulence (Rak et al 2019) can be used as a natural tracer (Fujita and Kunita 2011) and image patterns caused by water surface undulations tend to be more visible by taking images from small depression angles. Space-Time Image Velocimetry (STIV) is designed to utilize the natural water surface pattern by obtaining images from a small depression angle, but avoids problems caused by low image resolution for the forward/backward directions in ortho-rectified images (Fujita et al 2007, Fujita et al 2019). Taking an image from a low depression viewing angle enables water surface velocity measurements, without requiring labor demanding tracer seeding. STIV was designed in order to measure a one-component, one-dimensional velocity distribution (Fujita et al 2007, Tsubaki 2017). STIV is not suited for measuring complex, two-dimensional flow features. Therefore, this study chose LSPIV as a measure for quantifying water surface velocity.

Here, I propose a method for overcoming the problem caused by large distortion in ortho-rectification by combining multi-camera LSPIV. The main concept of the method, schematically illustrated in Figure 2 is recording images of an identical area of the water's surface from different locations and estimating the velocity field of each viewing angle. Then, the two-component, two-dimensional velocity field is reconstructed, with better accuracy, using velocity component data obtained from several viewing angles. The work presented focuses on obtaining the mean velocity field as primary velocity data that is not always available in environmental observations due to the restrictions attributed to field measurements.

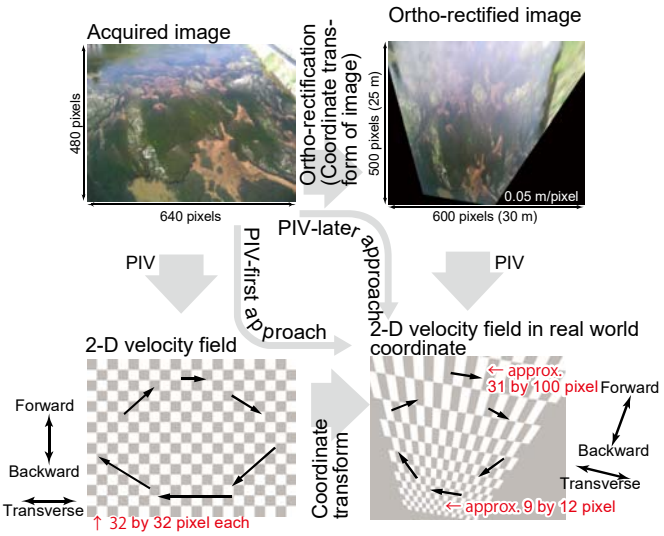


**Figure 1.** The procedures of LSPIV. Ortho-rectification is used in the normal LSPIV (PIV-later approach, clock-wise in the figure), but the 2-D velocity field in real world coordinates can be obtained using the coordinate transform of vectors estimated in the image coordinate (the PIV-first approach, counter-clock-wise in the figure).

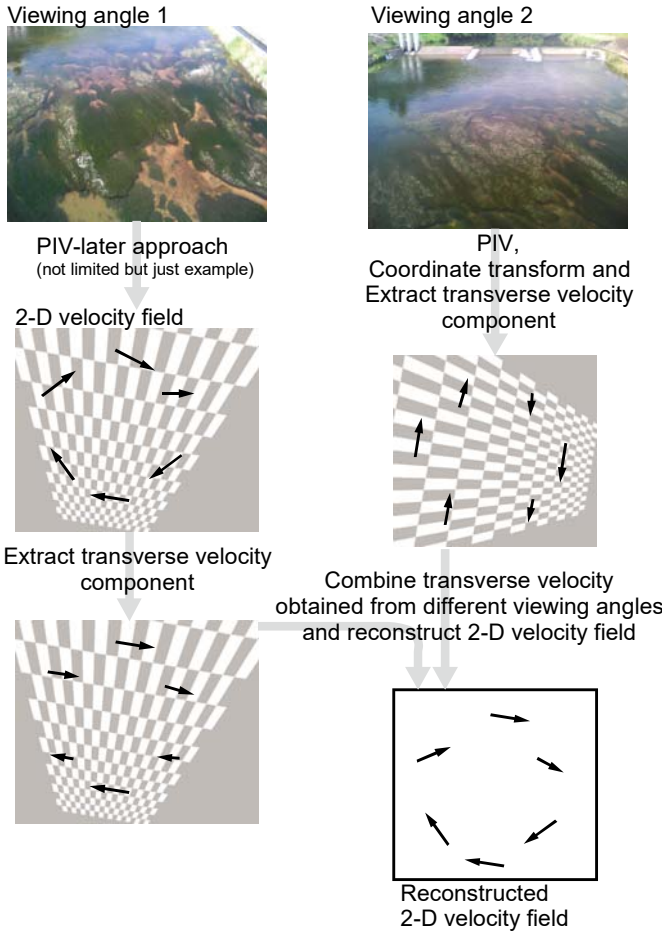


**Figure 2.** A schema of the proposed method. The transverse velocity component is calculated for each viewing angle and then the 2-D velocity field is reconstructed by combining the transverse velocity fields.

## 2. Method

The method proposed in this study incorporates a least squares algorithm. The procedures are as follows. The *i*-direction component of vector $\boldsymbol{b}$ as $\boldsymbol{a}_i$ (see Figure 3 for the geometric explanation) is defined. For a case where $\boldsymbol{b}$ is unknown, $\boldsymbol{b}$ may be reconstructed from an observed $\boldsymbol{a}_i$ s (i.e. the transverse component of a LSPIV measurement of the camera angle *i*). The square error of unknown $\boldsymbol{b}$ and observed $\boldsymbol{a}_i$ s may be estimated using:

$$\sum_i \left( \frac{\boldsymbol{a}_i \cdot \boldsymbol{b}}{|\boldsymbol{a}_i|} - |\boldsymbol{a}_i| \right)^2 . \tag{1}$$

By decomposing the vectors using the components (e.g. $\boldsymbol{b} = (b_x, b_y)$), equation (1) becomes:

$$\begin{aligned} &\sum_i \left( \frac{a_{i,x} b_x + a_{i,y} b_y}{|\boldsymbol{a}_i|} - |\boldsymbol{a}_i| \right)^2 \\ &= \sum_i \left( \left( \frac{a_{i,x} b_x + a_{i,y} b_y}{|\boldsymbol{a}_i|} \right)^2 - 2\left( a_{i,x} b_x + a_{i,y} b_y \right) + |\boldsymbol{a}_i|^2 \right). \end{aligned} \tag{2}$$

Components $b_x$ and $b_y$ can then be calculated based on equation (2) using the least squares approach. Therefore, the calculation consists of equation (2) differentiated with $b_x$ or $b_y$ equal to zero, namely:

$$0 = 2b_x \sum_i \left( \frac{a_{i,x}^{\ 2}}{|\boldsymbol{a}_i|^2} \right) + \boldsymbol{b}_y \sum_i \left( \frac{2a_{i,x}a_{i,y}}{|\boldsymbol{a}_i|^2} \right) + \sum_i \left( -2a_{i,x} \right) \quad \text{and} \tag{3}$$

$$0 = 2b_y \sum_i \left( \frac{a_{i,y}^{\ 2}}{|\boldsymbol{a}_i|^2} \right) + \boldsymbol{b}_x \sum_i \left( \frac{2a_{i,x}a_{i,y}}{|\boldsymbol{a}_i|^2} \right) + \sum_i \left( -2a_{i,y} \right). \tag{4}$$

By simultaneously solving equations (3) and (4), the two-componet velocity vector $\boldsymbol{b} = (b_x, b_y)$ can be calculated.

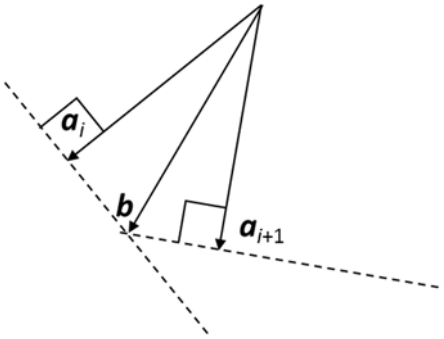


**Figure 3**. The relationship between vectors $\boldsymbol{b}$ and $\boldsymbol{a}_i$ s.

## 3. Validations

Two types of validation were conducted in order to explore the performance of the proposed method. The first validation was an assesment of the velocity distribution of a rigid rotating disk, as a fundamental and simplified situation. The second validation was the velocity reconstruction of the circulatory surface flow generated within an experimental flume.

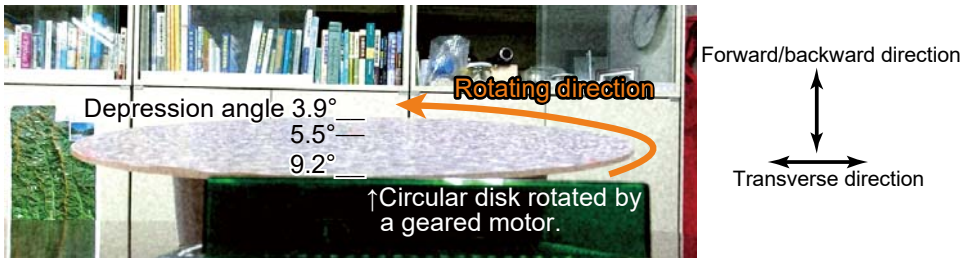


**Figure 4**. A sample image from the rotating disk movie. A smoothed Gaussian noise pattern was pasted on a rigid circular disk of 0.25 m in diameter. The disk was rotated at a constant angular velocity by a geared motor placed under the disk.

### *3.1 Rigid rotating disk experiment*

A video camera (HDR-CX390, Sony Corp.) was used to record a movie of a rotating disk from a small depression angle (ranging from 3.9° to 9.2°). Figure 4 shows a snap-shot of a recorded movie. The depression angle is small and the surface pattern is strongly distorted (the scale for the forward/backward direction of the disk is 1/10th of the transverse scale). The velocity field calculated by a river flow image obtained from such a viewing angle generally contains a non-negligible error. Thus, artificial image noise (the 'Noise HLS auto' filter in Adobe Premiere Pro CS6) was applied in order to mimic the

deformation of the water surface pattern found in actual rivers (see the discussion on experimental conditions in Tsubaki 2019). Velocity components obtained from the degraded movie were then combined in order to reconstruct the two-dimensional velocity field.

### *3.1.1 Velocity distributions calculated from the degraded movie*

Figure 5 shows the correlation between location and the velocity component calculated from the movie containing artificial noise. Both location and velocity components are normalized by the radius of the disk, $r$. The slope of the point cloud in the figure corresponds to the angular velocity. Both positive and negative deviation was confirmed in the $v$-$x$ correlation plot (the left panel of Figure 5). However, the $u$-$y$ plot displays a trend of underestimation for the velocity magnitude. The plot of Case PIV2 was scattered around $u = 0$ in the area far from the camera. Error found on the far side of the disc in Case PIV2 may be due to the largely skewed pattern of the surface caused by a small depression angle. To validate the approach proposed in Section 2, this velocity distribution was used.

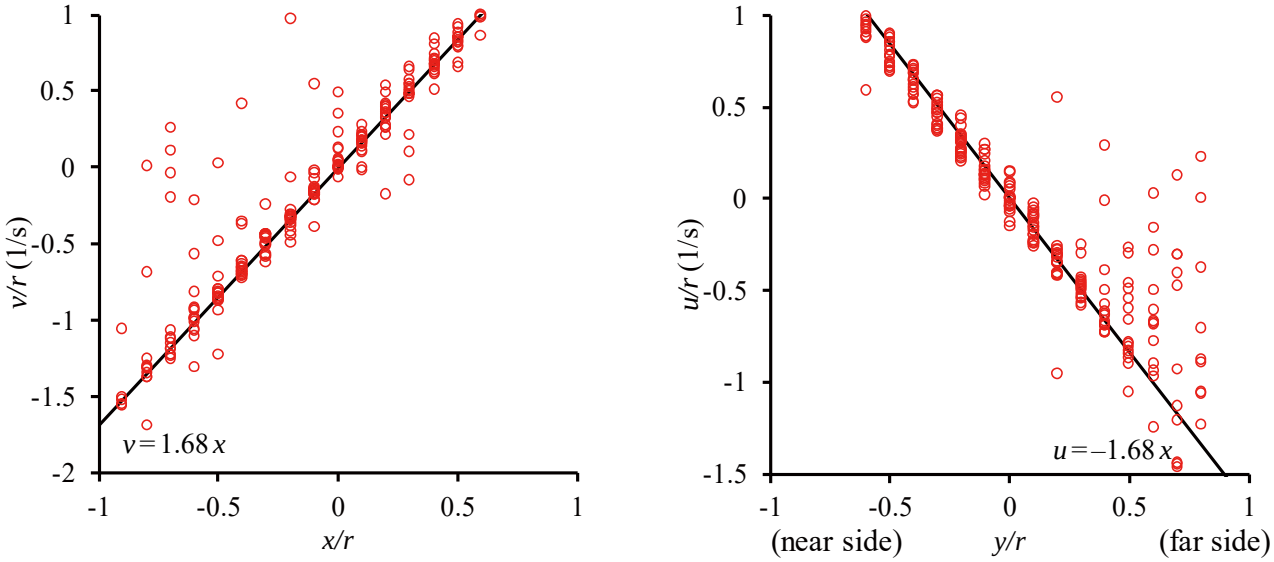


**(a)** $x$-$v$ correlation **(b)** $y$-$u$ correlation

**Figure 5**. The location-velocity component correlations of the velocity distribution obtained from the movie with artificial noise. Both the location and velocity were normalized by the radius of the disk. The solid lines correspond the velocity distribution based on the angular velocity of the disk. A series of ortho-rectified images was generated and then the PIV was applied (the PIV-later approach).

### *3.1.2 Validation of the velocity reconstruction method*

In the proposed method, the two-dimensional velocity field is reconstructed from velocity components for a different direction. Figure 6a explains two pairs of viewing camera angles, a pair different by 45° and a pair different by 90°. The velocity component transverse from the camera view (thick-solid vetctors in Figure 6b) is extracted from the 2D velocity obtained by the PIV (thin-dashed vectors in Figure 6b). To generate pairs of camera images (Figure 6a), the velocity distribution is rotated 45° and 90°. In Figure 7, the location-velocity correlations of the velocity fields reconstructed from the 45° and 90° pairs are plotted (open circles and plus symbols). Correlation of the original PIV result is also plotted as a reference (open circles).

Deviation from the regression line (not shown for simplification) is slightly reduced in both the 45° and 90° pairs, and the 90° pair appears to have the smallest deviation from the regression line. Quantitatively, the determination coefficients, $R^2$, for the $x$-$v$ correlation are 0.91, 0.79, and 0.88 for the 90° pair, the 45° pair, and the normal PIV, respectively. For the $y$-$u$ correlation, the $R^2$ are 0.92, 0.92, and 0.88 for the 90° pair, the 45° pair, and the normal PIV, respectively. In Figure 8, two-dimensional velocity distributions for the three cases are compared. The original PIV result (thin-dashed vectors) displays a reasonable velocity distribution in the area near the camera ($y/r < 0$). However, the velocity vector scatters on the far side of the disk ($y/r > 0.3$). The scatter of velocity distributions on the far side of the disk is reduced and the distribution becomes much more reasonable in plots of the 45° pair, especially for the 90° pair. Thus, a pair consisting of roughly a 90° difference in direction for the velocity component would be better for reconstructing the velocity distribution.

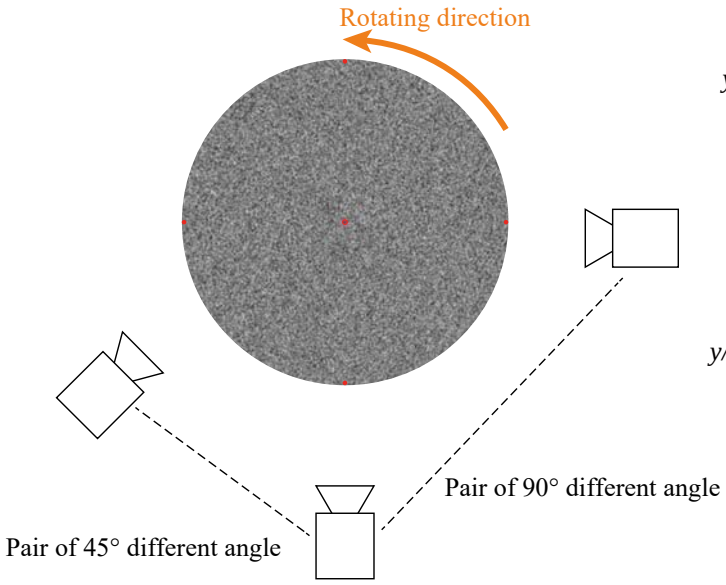


**(a)** Schematic plan view of two pairs of cameras with different 45° and 90° angles.

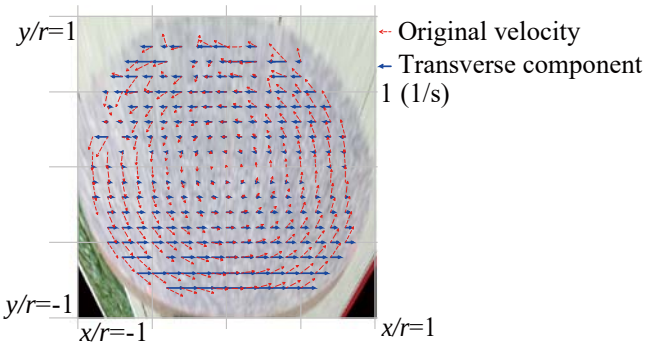


**(b)** Distribution of the transverse velocity component (thick-solid vectors) extracted from the original velocity distribution (thin-dashed vectors).

**Figure 6**. The combination of cameras making the pair of 45° and 90° angles (panel **a**) and the extracted transverse velocity component distribution (panel **b**).

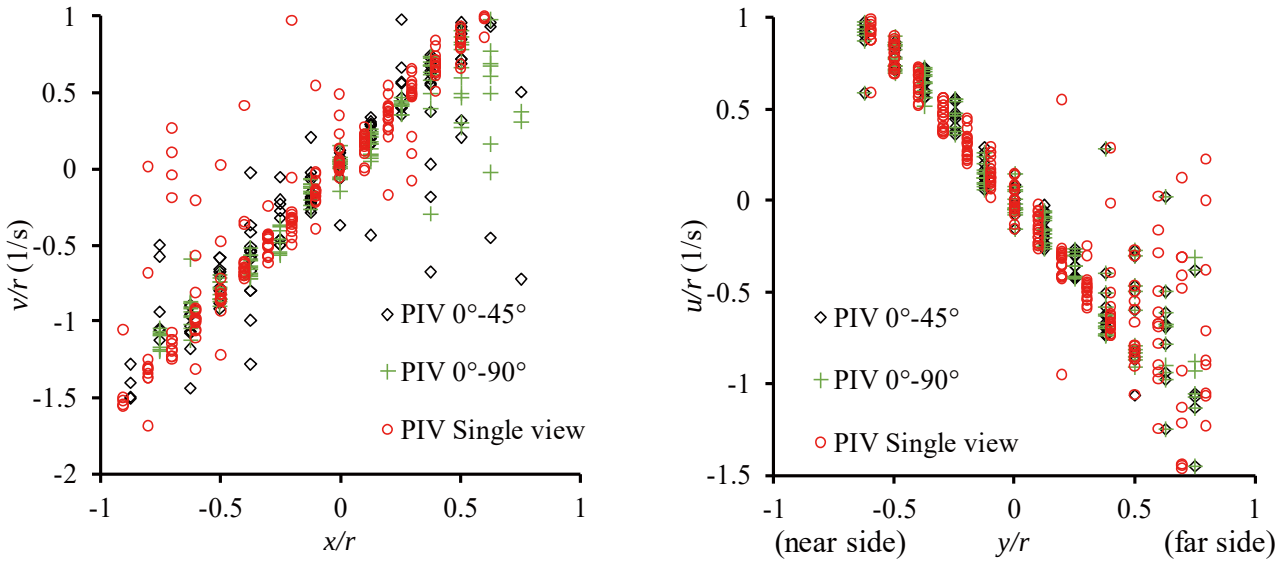


**(a)** *x*-*v* correlation **(b)** *y*-*u* correlation

**Figure 7**. The location-velocity component correlations of the velocity distribution reconstructed from the transverse velocity components of the 45° and 90° difference depicted by the open rhombus and the plus symbol, respectively.

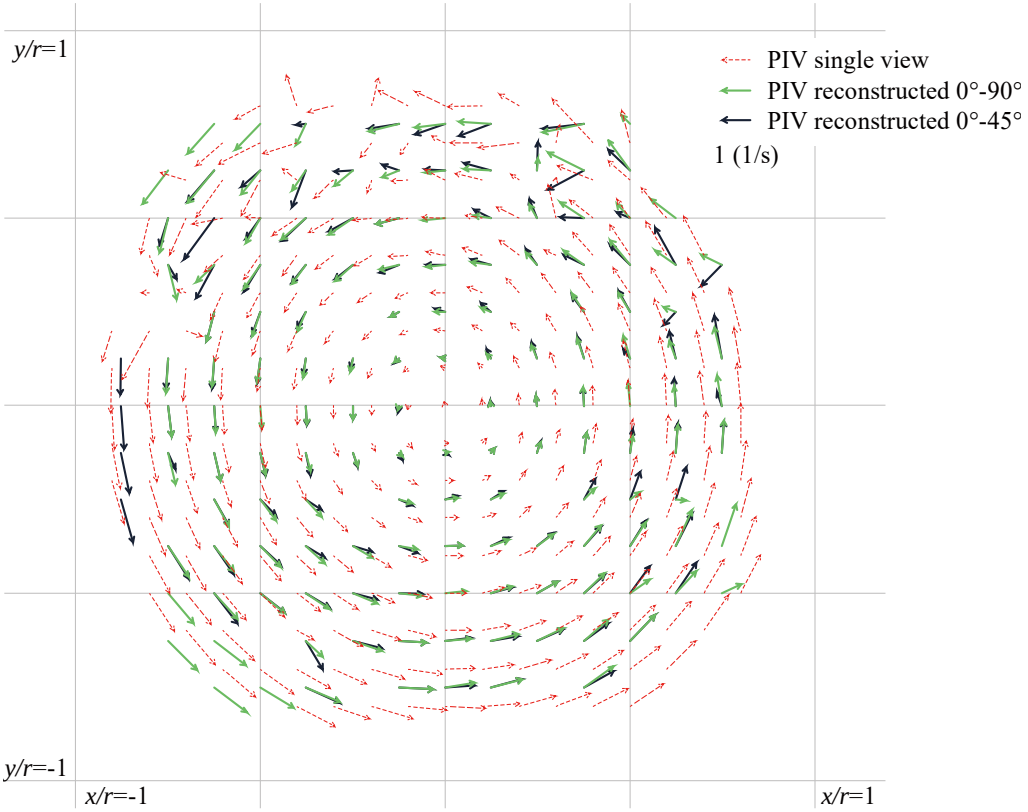


**Figure 8**. The two-dimensional velocity distribution and flow fields reconstructed from the 45° and 90° pairs.

### *3.2 Circulatory flow experiment*

For the circulatory flow experiment, a container in which the inner dimension was 0.42 by 0.32 by 0.19 $m^3$ was filled with water coloured with black acrylic pigment. Water in the container was driven by a jet flow made by a small electric pump located at the bottom corner of the container to make circulatory flow. After running the pump over ten minutes to make the flow turbulent but steady, sawdust was seeded onto the black coloured water surface as a surface flow tracer. Figure 9 shows the experimental setup. To take images of 1920 by 1080 pixels with 60 frames-per-second from the top, the digital video recorder (HDR-CX390, Sony Corp.) was used and the velocity field obtained from this large depression angle image was used for better and accurate results. Two cameras, HAS-L1 (DITECT Co. Ltd.), were set for taking low depression angle images (1024 by 768 pixels, 100 frames-per-second) with different horizontal viewing angles. A polystyrene foam board (0.364 by 0.258 by 0.002 $m^3$) was used to ortho-rectify the water surface between image recording sessions. Over 500 frame pairs with 20 frames-per-second were used in order to obtain a mean velocity field for each viewing angle. The velocity distribution was calculated by applying PIV to the recorded images and then the obtained velocity vectors were coordinate transformed (using the PIV-first approach).

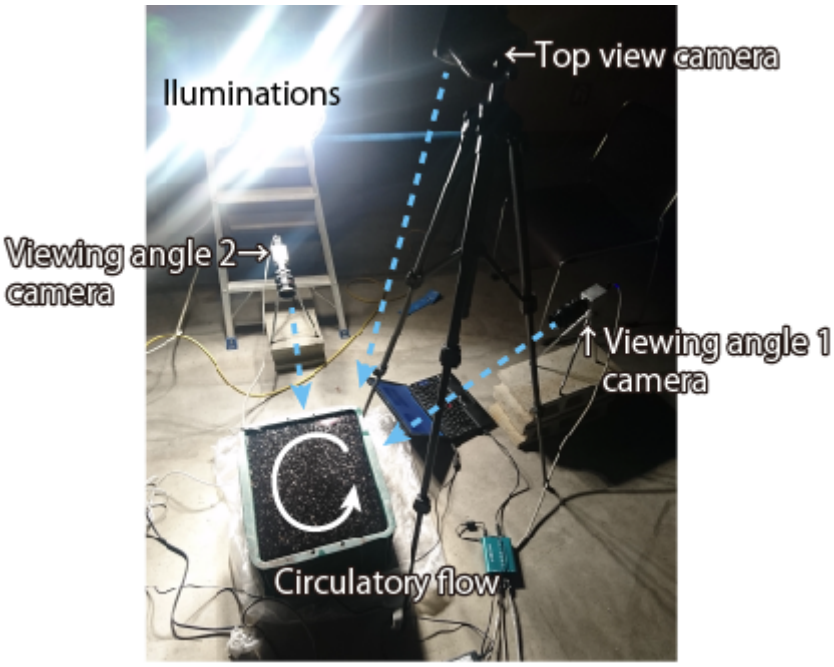


**Figure 9**. The setup for the circulatory flow experiment. The depression angle for viewing angles 1 and 2 were approximately 18° and 14°, respectively.

### *3.2.1 Velocity field comparison*

Figure 10 compares velocity fields obtained from image sets taken from different angles and reconstructed using the results of viewing angles 1 and 2. The red vectors show LSPIV results for images taken from the top of the flume. This viewing angle can record the water surface image with limited image distortion, making the image resolution suitable for the entire measurement domain. The velocity field obtained from the image taken from the top is regarded as a reference (correct one).

Velocity fields estimated from images taken from low depression angles (the blue and green vectors in Figure 10) show systematic error in the area far from the camera. The two regions of the velocity field are enlarged with dashed-line circles (a) and (b) in Figure 10. In region (a) enlarged in the figure, the flow direction is almost parallel to viewing angle 2 and normal to viewing angle 1. The velocity magnitude of viewing angle 2 (the green vector) seems overestimated as compared to the red vector (the reference), and the direction of viewing angle 1 (the blue vector) is oriented to be normal to viewing angle 1. Both errors are caused by strong inhomogeneity in the spatial resolution predominant for the case of low depression angle image capturing. Both errors are well mitigated in the reconstructed velocity and good agreement with the reference vector is observed.

The enlarged region (b) in Figure 10 shows a similar result. Thus, the direction of velocity viewing angle 2 (the green vector) seems biased as normal to viewing angle 2, and the blue vector contains errors in magnitude and direction. The reconstructed vector contains an error in magnitude but the direction is almost identical to the direction of the reference vector.

### *3.2.2 Velocity component statistics*

By assuming the LSPIV result based on the top view image as the reference, the statistics of velocity error are calculated. Figure 11 shows the determination coefficient, $R^2$, of velocity components $u$ and $v$ for the three velocity fields (viewing angle 1, viewing angle 2, and the velocity reconstructed from viewing angles 1 and 2). The reconstucred velocity shows the highest value of the $R^2$, while viewing angle 1 shows almost the same but a slightly lower $R^2$. Viewing angle 2 displays the lowest $R^2$. The depression angle of viewing angles 1 and 2 are 18° and 14°, respectively, which means the image taken from viewing angle 2 contains a larger image deformation, may limit the accuracy of the calculated velocity components, and may have caused the lowest $R^2$.

Figure 12 compares the root mean square error of the velocity direction anomaly based on the velocity direction of the top view LSPIV. The reconstructed velocity field shows less than half of the RMSE as compared to the single image LSPIV with low depression angles (viewing angles 1 and 2).

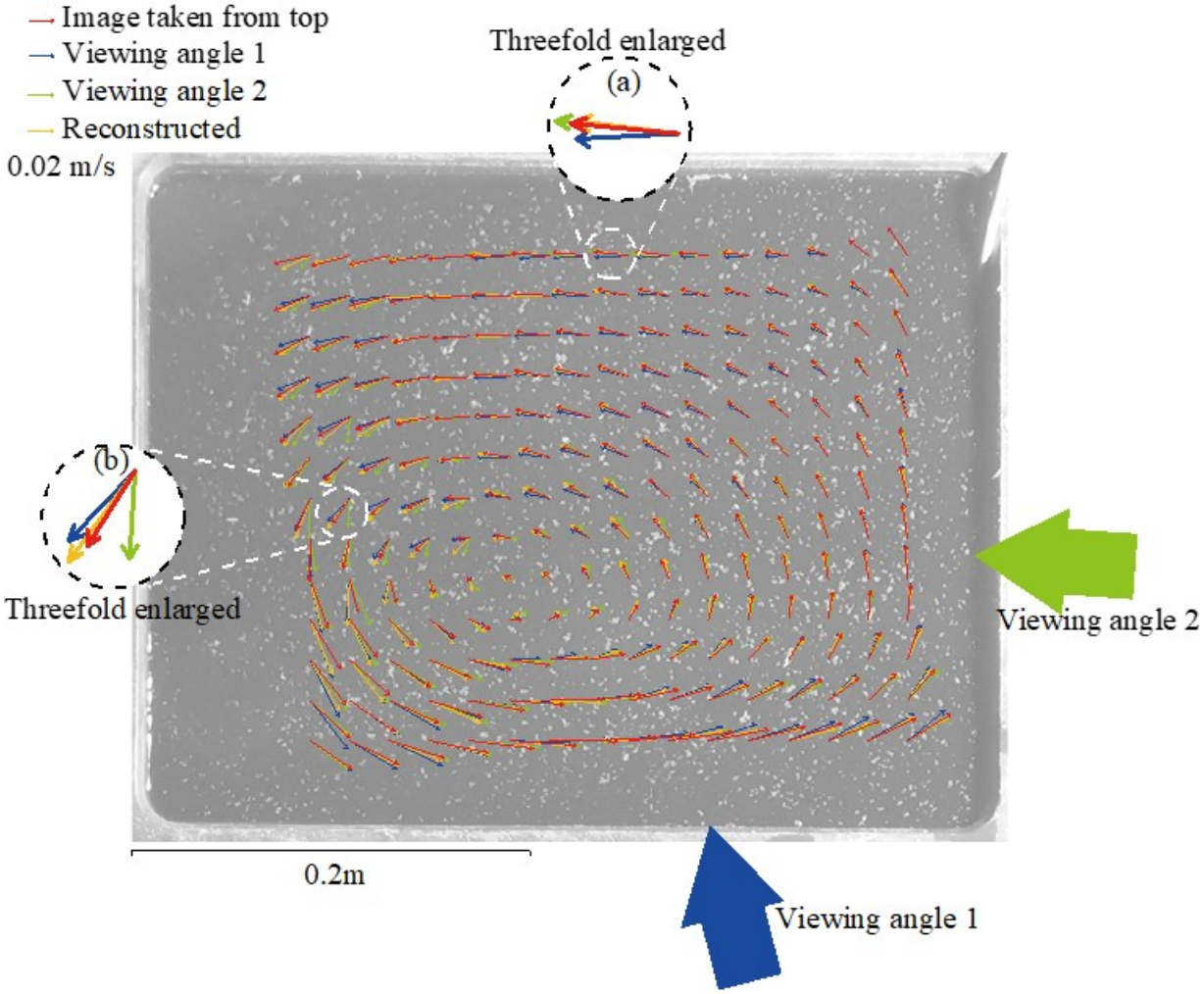


**Figure 10**. Velocity vectors of LSPIV from the image taken from the top (red arrows), viewing angle 1 (blue arrows, image taken from the bottom in the figure), viewing angle 2 (green arrows, image taken from the right), and the velocity reconstructed from viewing angles 1 and 2 (orange arrows).

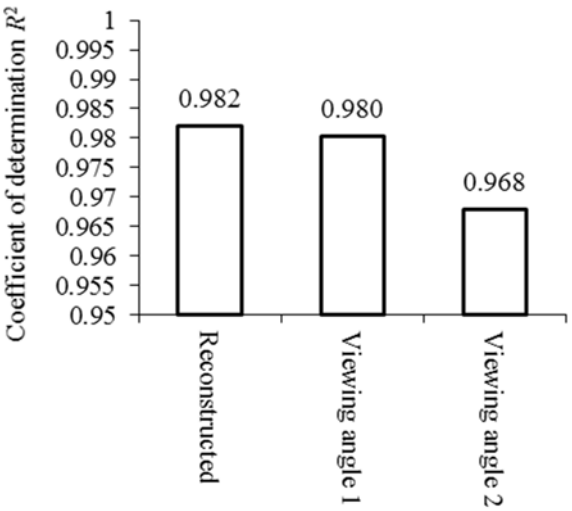


**Figure 11**. The coefficients of determination ($R^2$) for the three velocity distributions.

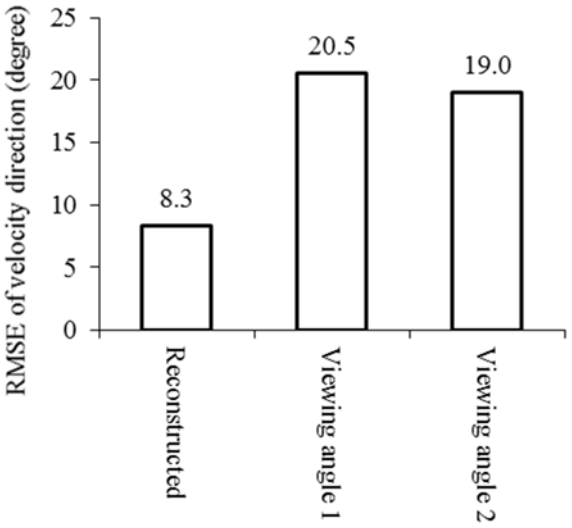


**Figure 12**. The root mean square error of the velocity direction for the three velocity distributions.

### *3.3 Summary in validation*

Two types of validation were conducted. From both the rigid rotating disk experiment and the circulatory flow experiment, erroneous velocities at the area far from the camera were mitigated by reconstructing the velocity field using two image angles. The coefficients of determination were also increased by combining two image angles. The RMSE of the velocity direction was reduced to less than half by reconstructing the velocity field in the circulatory flow experiment, implying that the suggested method would be suitable for reconstructing streamlines from accuracy-limited velocity fields calculated from low depression angle images obtained from different horizontal viewing angles.

## 4. Field Application

A LSPIV survey was conducted in order to clarify the large-scale vortex structure formed at a river section. The width of the section was approximately 200 m and images were obtained from two viewing angles located on the right side of a river bank. Surveillance image acquisition systems were used in order to capture and record images at each viewing angle. The frames were not synchronised. The depression angles of the image surrounding the focused area were approximately 1.5° and 2.0°. Due to the quite small depression angle and strong image and coordinate distortions, the two-dimensional velocity fields obtained by standard LSPIV seemed strongly biased (aligned normal to the viewing angles), and this circulatory flow was not visible from the standard LSPIV results (Figure 13a, the PIV-first approach was used). Transverse velocity components for both viewing angles were calculated. The velocity distribution was reconstructed by combining velocity data and plotted using the red vectors shown in Figure 13b. Flow separation on the left side bank can be confirmed based on the reconstructed velocity field. This flow feature corresponds well to the manual observation from a boat during the event.

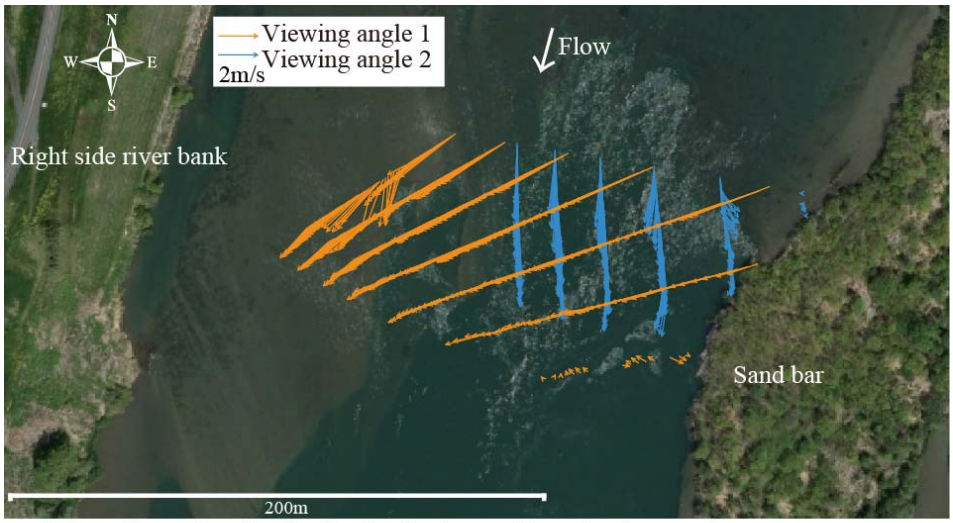


**a)** Two-dimensional velocity distributions of two viewing angles

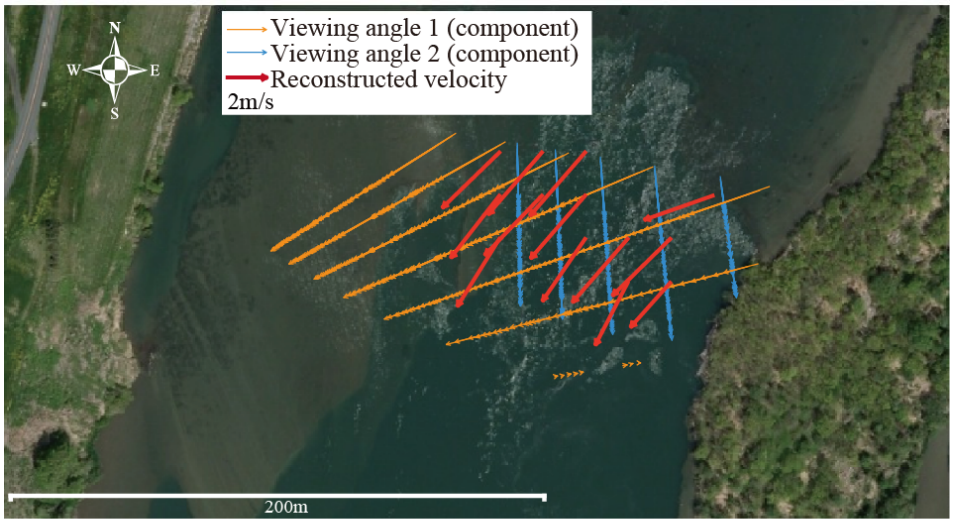


**b)** Transverse velocity components of two viewing angles and velocity distribution reconstructed from these velocity components

**Figure 13**. Two-dimensional velocity distributions of two viewing angles obtained from the river bank (panel **a**), and the extracted transverse velocity components of the 2D velocity of the above angles and the reconstructed velocity distribution (panel **b**). (Background photo source: Geospatial Information Authority of Japan website (https://maps.gsi.go.jp/#18/35.336885/136.748128/&ls=_ort).

## 5. Conclusions

In this study, I proposed a new method for reconstructing the two-dimensional velocity distribution, with better accuracy, from a set of accuracy limited velocity fields calculated from images obtained from multiple viewing angles. Basic characteristics of error in velocities calculated from low depression angle images from a rotating disk experiment and a flume experiment were investigated. The proposed method was applied to field measurements where the standard LSPIV does not work well for extracting flow features due to very low depression angles. The flow feature was successfully extracted using the proposed method.

The proposed method is simple and may leave room for improvement. Further fundamental investigations regarding uncertainty in LSPIV based on images obtained from small depression angles are needed. Based on such quantitative uncertainty estimations, a more sophisticated but robust velocity field reconstruction method will be developed.

This study focused on obtaining the mean velocity field. However, the proposed method is also applicable to reconstructing the instantaneous velocity field from multiple cameras. In this study, the mean velocity field was a focus due to the limited understanding of uncertainty for the measurement discussed. To apply the proposed method for instantaneous velocity field reconstruction, careful discussions surrounding uncertainty for the instantaneous velocity field obtained from each viewing angle are required (Sciacchitano 2019). Such an approach, incorporated with STIV, would be another promising study direction. The method was applied in order to analyze environmental flow but can be utilized for image velocimetry of the flow field where the optical configuration is substantially restricted (e.g. in-vivo imaging or flow in/around complicated structures).

## Acknowledgements

The study was conducted under collaborative support from the Chubu Regional Development Bureau of the Ministry of Land, Infrastructure, Transport and Tourism, Japan. Support from and communication with affiliates of the above bureaus are deeply appreciated. The work was partially funded by: (1) the Foundation of River & Basin Integrated Communications, Japan, and (2) JSPS KAKENHI, grant JP17K06574.

## References

[1] Sciacchitano A 2019 Uncertainty quantification in particle image velocimetry *Meas. Sci. Technol.* **30** 092001
[2] Scharnowski S et al 2019 On the universality of Keane & Adrian's valid detection probability in PIV *Meas. Sci. Technol.* **30** 035203
[3] Fujita I et al 2019 *E-proceesings of the 38th IAHR World Congress*, doi:10.3850/38WC092019-0652
[4] De Schoutheete F et al 2019 *E-proceesings of the 38th IAHR World Congress*, doi:10.3850/38WC092019-0782
[5] Rak G et al 2019 *E-proceesings of the 38th IAHR World Congress*, doi:10.3850/38WC092019-5553
[6] Kim Y et al 2008 *Water Resources Research* **44**.9
[7] Fujita I et al 2004 Velocity measurements around non-submerged and submerged spur dykes by means of Large-Scale image velocimetry, *Journal of Hydroscience and Hydraulic Engineering* **22**, No. 1, 51–61.
[8] Fujita I & Kunita Y 2011 Application of aerial LSPIV to the 2002 flood of the Yodo River using a helicopter mounted high density video camera, *Journal of Hydro-environment Research* **5**.4, 323–331.
[9] Fujita I et al 2007 Development of a non−intrusive and efficient flow monitoring technique: The space-time image velocimetry (STIV). *International Journal of River Basin Management* **5**.2, 105–114.
[10] Tsubaki R 2017 On the Texture Angle Detection Used in Space‐Time Image Velocimetry (STIV). *Water Resources Research* **53**.12, 10908–10914.
[11] Bento A M et al 2017 Direct Estimate of the Breach Hydrograph of an Overtopped Earth Dam, *Journal of Hydraulic Engineering* **143**.6, doi: 10.1061/(ASCE)HY.1943-7900.0001294.
[12] Johnson E D & Cowen E A 2017 Estimating bed shear stress from remotely measured surface turbulent dissipation fields in open channel flows, *Water Resources Research* **53**, 1982–1996, doi:10.1002/2016WR018898.
[13] Strobl B et al 2019 Accuracy of crowdsourced streamflow and stream level class estimates, *Hydrological Sciences Journal*, DOI: 10.1080/02626667.2019.1578966
[14] Tauro F et al 2017 Streamflow observations from cameras: Large-Scale Particle Image Velocimetry or Particle Tracking Velocimetry? *Water Resources Research* **53**.10, 10374–10394.
[15] Tauro F et al 2018 Optical sensing for stream flow observations: A review. *Journal of Agricultural Engineering* **49**.4, 199–206. https://doi.org/10.4081/jae.2018.836
[16] Tsubaki R et al 2015 Large-scale particle image velocimetry (LSPIV) implementation on smartphone, *Proceedings of 36th IAHR Congress*, ISBN: 978-90-824846-0-1, Paper number 3874 on WEB site, Hague, Netherlands.
[17] Tsubaki R et al 2018 LSPIV app data fusion of velocity and elevation data, *Proceedings of 12th International Symposium on Ecohydraulics*, Tokyo, Japan.
[18] Tsubaki R et al 2019 Multi-camera Large-Scale Partice Image Velocimetry, *Proceedings of 38th IAHR Congress*, doi:10.3850/38WC092019-1364, Panama City, Panama.
[19] Hauet A et al 2008 Experimental system for real-time discharge estimation using an image-based method *J. Hydrologic Eng.* **13**.2 105–110